analytical chemistry

Article

Cite This: *Anal. Chem.* 2018, 90, 9125–9131

pubs.acs.org/ac

Visualizing miR-155 To Monitor Breast Tumorigenesis and Response to Chemotherapeutic Drugs by a Self-Assembled Photoacoustic Nanoprobe

Wenhua Cao, Wen Gao,* Zhenhua Liu, Wenjing Hao, Xiang Li, Yuhui Sun, Lili Tong, and Bo Tang*

College of Chemistry, Chemical Engineering and Materials Science, Collaborative Innovation Center of Functionalized Probes for Chemical Imaging in Universities of Shandong, Key Laboratory of Molecular and Nano Probes, Ministry of Education, Institute of Biomedical Sciences, Shandong Normal University, Jinan 250014, P.R. China

Supporting Information

ABSTRACT: MicroRNA-155 (miR-155), which facilitates breast tumor growth and invasion by promoting tumor cell proliferation and inhibiting cell apoptosis, is considered an ideal early diagnostic and prognostic marker. Herein, we developed a self-assembled hybridization chain reaction (HCR)-based photoacoustic (PA) nanoprobe for highly sensitive in situ monitoring of dynamic changes in miR-155 expression during breast tumorigenesis and chemotherapy. The PA nanoprobes (Au-H1/PEG and Au-H2/PEG) were constructed by linking poly(ethylene glycol) (PEG) and two hairpin DNA strands (H1 and H2, respectively) to the surface of gold nanoparticles (AuNPs). In the presence of miR-155, the PA nanoprobes self-assembled into Au aggregates via HCR between H1, H2, and miR-155. The decreased interparticle distance in these aggregates enhanced the surface plasmon resonance (SPR) in the AuNPs. Consequently, the absorption peak of the PA nanoprobes red-shifted, and strong PA signals were generated. This strategy enabled the sensitive and quantitative detection of miR-155 with a low detection limit of 0.25 nM. As a result, PA signals of miR-155 were captured on the second day after tumor inoculation when the solid tumor had not yet formed. Dynamic changes in miR-155 during tumor growth and chemotherapy were also monitored in real time to assess the therapeutic effects via PA imaging. By virtue of these advantages, the PA nanoprobes may provide a powerful platform for in situ detection of miR-155 and thus real-time monitoring of tumorigenesis and drug response in breast cancer.

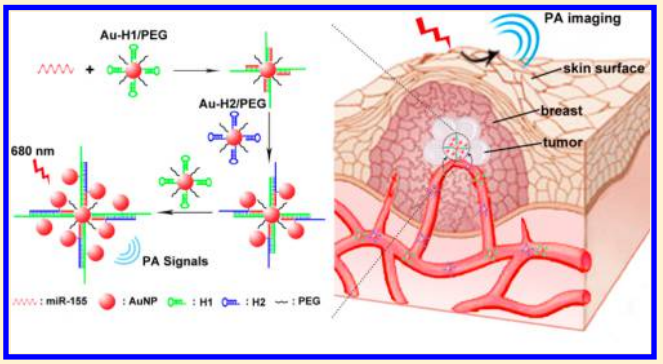

Breast cancer is the most commonly diagnosed form of cancer for women worldwide and is highly lethal. Due to its inconspicuous early symptoms, breast cancer is typically diagnosed during middle or late stages, increasing the risk of metastasis and distant recurrence, which can make it incurable.[1] Therefore, the early diagnosis and therapy of breast cancer is key to improving survivability.[2,3] MicroRNAs (miRNAs) are a type of noncoding RNAs that control gene expression by targeting mRNAs and eventually leading to translation repression or RNA degradation.[4] Thus, miRNAs play an important role in various cellular processes, and their aberrant expression is closely correlated with multiple cancers.[5−11] Specifically, miRNA-155 (miR-155), an oncogenic miRNA, is overexpressed in breast cancer cells. It facilitates tumor growth and invasion by promoting tumor cell proliferation and inhibiting apoptosis.[12,13] Its expression is pivotal to understand the tumorigenesis, progression, and prognosis.[14,15] Therefore, miR-155 has become an ideal biomarker candidate for diagnosing and monitoring malignant breast tumors and assessing therapeutic effects.[16]

Recently, many strategies, including Northern blotting, microarray analysis, quantitative real-time polymerase chain reaction (qRT-PCR), and fluorescence probes have been developed for miRNA detection and quantification with superior specificity and sensitivity.[11,17−23] They can be used to detect miRNAs at both the cellular and organ levels. However, cell and organ isolation used in these studies is not representative of the complex in vivo environment. Additionally, distinguishing unformed tumors from normal tissues is difficult, which makes isolating tumor tissue from the body impossible during the early stages of breast cancer. Although fluorescence probes enable detection of miRNA in living cells and in vivo, the interference of tissue autofluorescence and the limitation of tissue penetration makes fluorescence imaging nonideal for in situ detection of miRNAs.[24] Moreover, miRNAs are expressed at less than 50 000 copies per cell.[25] This low abundance limits in situ detection. In addition, when foreign substances enter the body, they are often eliminated quickly by the reticuloendothelial system (RES).[26,27] To detect traces of miR-155, most of the probes should be able to easily

Received: April 5, 2018
Accepted: July 2, 2018
Published: July 2, 2018

DOI: 10.1021/acs.analchem.8b01537
Anal. Chem. 2018, 90, 9125−9131

enter the tumor site and remain there for a long time. Therefore, to successfully detect miR-155 in situ, the detecting platform must satisfy the following criteria: (1) deep tissue penetration and weak background noise, (2) high sensitivity and selectivity, and (3) high in vivo stability and enhanced penetration and retention (EPR) effect.

As an emerging imaging modality, photoacoustic (PA) imaging combines optical and ultrasound imaging technologies and converts pulsed lasers into ultrasound signals. It overcomes the limited deep tissue penetration associated with fluorescence imaging and shows higher contrast and better spatial resolution.[28,29] Therefore, PA imaging is ideal for in situ detection. To better amplify the PA signal, a hybridization chain reaction (HCR) can be used, which can achieve highly sensitive detection of initiator strands through a triggered self-assembly process between the initiator strands and two stable hairpin DNAs.[22,30,31] Based on these methods, we report here the first realization of a self-assembled HCR-based PA nanoprobe for the highly sensitive in situ detection of miR-155 during breast tumorigenesis and chemotherapy. Two thiol-terminated single-strand DNAs (H1 and H2), which could form hairpin structure, were designed and linked to gold nanoparticles (AuNPs) through Au−thiol (Au−S) bonds. To improve the stability and biocompatibility of the PA nanoprobes, thiol-terminated PEG was also conjugated onto the surface of the AuNPs. In the absence of miR-155, the UV absorption peak of the PA nanoprobes was located at 528 nm with no detectable PA signals. When the PA nanoprobes reached the tumor site via the EPR effect, they self-assembled into Au aggregates via HCR between H1, H2, and overexpressed miR-155. The decreased interparticle distance in these aggregates enhanced the surface plasmon resonance (SPR) in the AuNPs.[32] Consequently, the maximum absorption peak red-shifted, and the self-assembled aggregates produced strong PA signals at 680 nm. Therefore, the "turned-on" PA nanoprobes achieved highly sensitive and selective detection of miR-155 with a low detection limit of 0.25 nM. For in situ PA imaging, PA signals of miR-155 were captured on the second day after tumor inoculation, when the solid tumor had not yet formed. The intensities of these signals were increased with the tumor development. In addition, the PA nanoprobes have monitored different responses to doxorubicin (DOX) treatment at different stages of tumor development. These results suggested that the PA nanoprobes were able to diagnose breast cancer early through visualizing miR-155 and monitor in real-time miR-155 expression during breast cancer growth and chemotherapy, both of which are helpful for further exploring the mechanism underlying the occurrence, development, and prognosis of breast cancer. A schematic of the self-assembled HCR-based PA nanoprobes for in situ PA detection of oncogene miR-155 is depicted in Scheme 1.

EXPERIMENTAL SECTION

Hybridization Chain Reaction. According to a previously reported method,[30] two thiol-modified single-strand DNAs were reduced by tris(2-carboxyethyl) phosphine (TCEP) at 37 °C for 1 h. Then, the mixture was incubated at 95 °C for 2 min and slowly cooled to room temperature for 1 h to ensure that the DNA perfectly folded into hairpin structures (H1 and H2). Next, H1 (1 μM) and H2 (1 μM) were mixed with different concentrations of miR-155 (0, 0.1, 0.33, 1, 3.3, or 10 μM) in SPSC buffer (50 mM Na_2HPO_4, 0.5 M NaCl, pH 7.4) and incubated for 4 h at room temperature. The results were analyzed by agarose gel electrophoresis (miR-155 and DNA sequences are shown in Table S1).

Scheme 1. Schematic of the Self-Assembled HCR-Based PA Nanoprobes for in Situ PA Detection of Oncogene miR-155

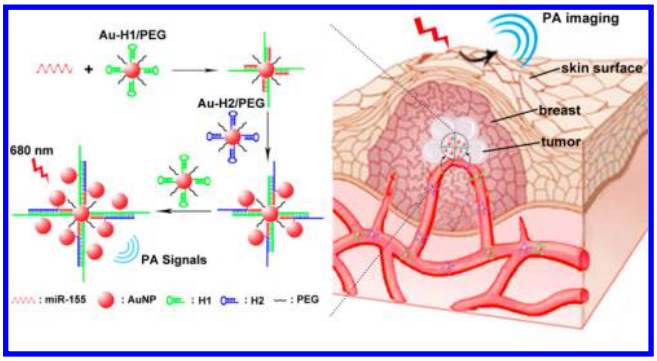

Synthesis of AuNPs. The AuNPs were synthesized using a modified trisodium citrate reduction method.[33] Briefly, a reaction mixture containing 1 mL of trisodium citrate (3% w/v) and 98 mL of ultrapure water was heated until boiling with vigorous stirring. Then, 1 mL of $HAuCl_4 \cdot 4H_2O$ (1% w/v) was quickly injected into the boiling solution under vigorous stirring, and boiling was maintained for 10 min before cooling on ice. The mixture was centrifuged (12 000 rpm, 10 min) at room temperature and washed three times with ultrapure water. The prepared AuNPs were stored at 4 °C, and their concentrations were determined by measuring their extinction at 522 nm ($\varepsilon = 2.7 \times 10^8$ L mol^{-1} cm^{-1}).

Preparation of PA Nanoprobes. Two samples (2 mL each) of phosphate buffered solution (PBS, 10 mM, 137 mM NaCl, pH 7.4) containing 3 nM AuNPs, 100 nM H1 or H2, and 100 nM HS-PEG (MW 1000) were shaken for 12 h at 37 °C. Then, a sodium dodecyl sulfate (SDS) solution (10%) was added into the mixture to achieve a 0.1% SDS concentration, and phosphate buffer (100 mM, pH 7.4) was added to a final concentration of 10 mM. The concentration of NaCl was slowly increased to 0.15 M by adding NaCl solution (2 M) over an 8 h period. The mixture was shaken for another 24 h and centrifuged (14 000 rpm, 10 min) at 4 °C. The final products (Au-H1/PEG and Au-H2/PEG) were washed three times with PBS to remove unreacted material and redispersed in PBS for further use. The single-base mismatched PA nanoprobes (Au-H1*/PEG and Au-H2*/PEG) were prepared as above. The details of the sequences are shown in Table S1 in the Supporting Information).

miR-155-Triggered Self-Assembly and PA Response of the Nanoprobes in Vitro. miR-155-triggered self-assembly was studied by mixing 100 nM of miR-155 or single-base mismatched DNA with 3 nM PA nanoprobes (Au-H1/PEG and Au-H2/PEG) in 2 mL of PBS buffer (10 mM, pH 7.4). The mixture was incubated at 37 °C for 4 h. Then, the products were purified from the redundant miR-155 by centrifuging (14 000 rpm, 10 min, and 4 °C) and redispersed in PBS. The results were analyzed by high-resolution transmission electron microscopy (HRTEM), UV−vis absorption spectroscopy, and dynamic light scattering (DLS). PA imaging of miR-155 was investigated by incubating 3 nM PA nanoprobes with different concentrations of miR-155 (0, 5, 10, 20, 40, 60, 80, or 100 nM) at 37 °C for 4 h. The absorption spectrum and the color of the solution were recorded. Then, the PA images were captured using an Endra Nexus128 PA

DOI: 10.1021/acs.analchem.8b01537
Anal. Chem. 2018, 90, 9125−9131

tomography system with a 680 nm pulse laser. For the optimum volume of PA nanoprobes, 10 nM miR-155 was incubated with different concentrations of PA nanoprobes (0, 10, 20, 30, 40, 50, 60, or 70 μg/mL) at 37 °C for 4 h. The PA signals at 680 nm were captured.

miR-155-Triggered Self-Assembly and PA Response of the Nanoprobes in Vivo. The self-assembly process of PA nanoprobes in living cells was first examined. The perfectly matched or single-base mismatched PA nanoprobes (50 μg/mL) were incubated with 4T1 cells (5×10^6 cells). After 1 and 4 h incubation, the cells were collected for the TEM analysis.[34] Then the self-assembly process in tumors was analyzed. The perfectly matched or single-base mismatched PA nanoprobes (dose = 25 mg/kg) were injected intratumorally into BALB/c mice bearing 4T1 orthotopic tumors[35] when the tumors reached approximately 100 mm^3. The tumors were harvested for TEM analysis 1 or 4 h after injection. Finally, the in vivo PA imaging was carried out on BALB/c mice bearing 4T1 orthotopic tumors (volume ≈ 100 mm^3) after intratumoral injection of perfectly matched and single-base mismatched PA nanoprobes (25 mg/kg). For comparison, the same amount of PA nanoprobes was injected into the muscle on the left leg of this mouse. Four hours after injection, these four groups of mice (n = 6) were anesthetized using 1.5% isoflurane in medical air at a flow rate of 2 L/min.[36] PA images were captured using an Endra Nexus128 PA tomography system with a 680 nm pulse laser.

Visualizing miR-155 To Monitor Breast Tumorigenesis by PA Nanoprobes. The PA nanoprobes were intravenously injected into BALB/c mice bearing 4T1 orthotopic tumors at different stages (0, 2, 4, 8, 12, 16, and 20 d postinoculation times) with a dose of 25 mg/kg. Then, the PA images were collected at 680 nm before injection and 8 h after injection. The relative PA intensity was quantified and calculated by subtracting the preinjection signal intensity from the PA intensity at 8 h postinjection. The mice administrated with the single-base mismatched PA nanoprobes were set as control group.

Visualizing miR-155 To Assess Chemotherapeutic Drug Efficacy by PA Nanoprobes. The BALB/c mice were inoculated with 4T1 orthotopic tumors and then randomly divided into four groups (n = 6). Group I was treated with doxorubicin (DOX) via intratumoral injection at 0 d postinoculation; group II was treated with DOX at 4 d postinoculation; group III was treated with DOX at 12 d postinoculation; the untreated group IV was set as a control. The dose of DOX is 0.5 mg/kg injected daily for 4 consecutive days. For monitoring tumor response to DOX, the PA nanoprobes were intravenously injected into these mice in each group at different stages (0, 2, 4, 8, 12, 16, and 20 d postinoculation times) at a dose of 25 mg/kg. Then, the PA images and relative PA intensity were collected and calculated as mentioned above.

RESULTS AND DISCUSSION

Preparation and Characterization of PA Nanoprobes. AuNPs were synthesized as previously reported with slight modifications. The HRTEM images showed that the spherical AuNPs were monodispersed in the aqueous phase with a diameter of approximately 25 nm (Figure 1a), which was consistent with the results determined using DLS (Figure 1f). Then, two thiol-terminated single-strand DNAs (H1 and H2) were specifically designed according to the sequence of miR-155.[13,30] After folding into hairpin structures, HCR occurred in the presence of miR-155, and the results were examined by agarose gel electrophoresis (Figure S1). Only one band of H1/H2 appeared with a small molecular weight (lane 7) in the absence of miR-155, suggesting that no HCR occurred. Comparatively, new bands appeared when H1 and H2 were incubated with various concentrations of miR-155, which indicated HCR had taken place to form a long double helix. Thus, the HCR enabled PA nanoprobes self-assembled into Au aggregates for the detection of miR-155. To construct the PA nanoprobes, H1, H2, and PEG were linked to the AuNPs through Au−S bonds, forming Au-H1/PEG and Au-H2/PEG, respectively. As shown in Figure 1b, the morphology or monodispersity did not obviously change after modification with DNA and PEG. However, the maximum absorption peaks of the AuNPs red-shifted from 522 to 528 nm (Figure 1e), and the hydrodynamic diameter changed from 24.36 to 28.21 nm (Figure 1f), confirming the formation of Au-H1/PEG or Au-H2/PEG. The successful fabrication of the PA nanoprobes was further verified by the ζ potential (Figure S2). The AuNPs displayed a negative potential (−26.6 ± 1.3 mV) owing to the citrate groups, and a higher negative charge (−35.4 ± 1.6 mV) was observed after modification with DNA and PEG. Thiol-terminated PEG, a commonly functionalized reagent, was used to improve AuNP stability and protect DNA from nuclease digestion.[37,38] As observed from Figure S3, PA nanoprobes modified with PEG remained stable in different solutions (water, PBS, Dulbecco's modified Eagle medium (DMEM) or serum freshly taken from healthy mice) after 7 days of incubation, while PA nanoprobes not modified by PEG aggregated into large particles. Moreover, the nuclease resistance stabilities of the PA nanoprobes were studied using deoxyribonuclease I (DNase I).[39] As shown by the gel electrophoresis results (Figure S4), pure H1 and the H1 on the Au-H1 were cleaved into small fragments in the presence of DNase I, whereas no small DNA fragments were produced after Au-H1/PEG were treated with DNase I. These results demonstrated that the PEG can effectively protect the hairpin DNA from enzyme degradation. Thus, the PA nanoprobes, with their high nuclease resistance and stability, can be used for in situ detection.

To verify the self-assembly of PA nanoprobes triggered by miR-155, the loading efficiencies of H1 and H2 were first

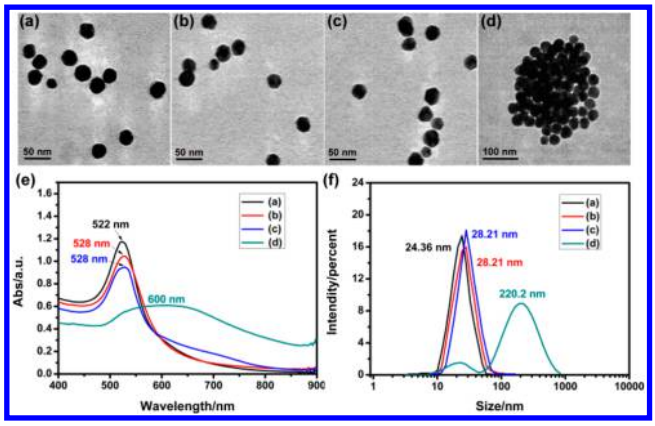

Figure 1. Characterization of the PA nanoprobes. HRTEM images of (a) AuNPs, (b) Au-H1/PEG + Au-H2/PEG, (c) Au-H1/PEG + Au-H2/PEG + single-base mismatched DNA, (d) Au-H1/PEG + Au-H2/PEG + miR-155. (e) UV−vis absorption spectra and (f) hydrodynamic diameters of the samples in panels a−d.

DOI: 10.1021/acs.analchem.8b01537
Anal. Chem. 2018, 90, 9125−9131

quantitated using a NanoDrop spectrophotometer. The average number of H1 or H2 loaded onto each AuNP was calculated to be 21 ± 1. The high loading efficacy ensures the self-assembly of nanoprobes via HCR between H1, H2, and miR-155. Then, miR-155 was incubated with the PA nanoprobes at 37 °C for 4 h. The color of the solution obviously changed from red to blue-violet (Figure S5), indicating the formation of Au aggregates.[32] HRTEM images and DLS further verified that the size of the resulting Au aggregates was approximately 220.2 nm (Figure 1d,f, blue line). The absorption peak also red-shifted to 600 nm (Figure 1e, green line), which was attributed to the enhanced SPR in the AuNPs. In comparison, single-base mismatched DNA was unable to initiate Au aggregate formation, as demonstrated by the lack of changes in the HRTEM image, UV−vis absorption spectrum, and DLS results (Figure 1c,e,f, respectively). These results suggested that the PA nanoprobes were triggered by miR-155 to assemble into Au aggregates, rather than nonspecifically aggregating, and thus, they can be used for the specific detection of miR-155.

In Vitro PA Response of Nanoprobes. To explore the possibility of using PA imaging for miR-155 detection, different concentrations of miR-155 (0, 5, 10, 20, 40, 60, 80, or 100 nM) were incubated with PA nanoprobes at 37 °C for 4 h. Obviously, the color of the solution gradually changed with the addition of miR-155 (Figure 2a). Moreover, there was a miR-155-concentration-dependent absorbance change for PA nanoprobes. As shown in Figure 2c, the peak located at 528 nm gradually decreased with the increasing of the miR-155 concentration, while a new broad absorption (550−700 nm) appeared and correspondingly increased. Then, PA imaging of the corresponding solution was carried out with a 680 nm pulse laser. The PA intensities increased with increasing concentration of miR-155 from 0 to 100 nM (Figure 2b,d). The quantization curve of the PA signals showed good linearity between the PA intensities and the miR-155 concentrations from 0 to 10 nM. The linear equation was $I = 42.313c + 66.358$ with the correlation coefficient of $R = 0.99644$, where I represents the PA intensity and c represents the concentration of the miR-155. The detection limit was determined to be 0.25 nM, which completely satisfied the requirement for in situ detection of miR-155.

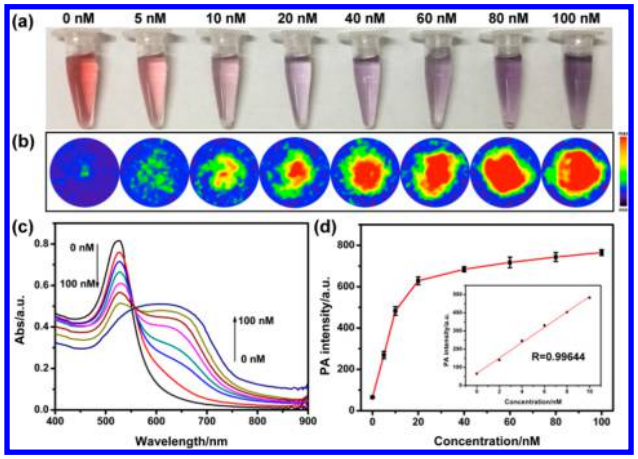

Figure 2. In vitro PA response of PA nanoprobes triggered by miR-155. (a) Photograph, (b) PA imaging, and (c) UV−vis absorption spectra of the nanoprobes incubated with different concentrations of miR-155 (0, 5, 10, 20, 40, 60, 80, and 100 nM). (d) Quantification of the PA intensity values in panel b. (inset) Calibration curve between the PA signals and the concentrations of miR-155 from 0 to 10 nM. Data are shown as mean ± SD of three independent experiments performed in duplicate.

Moreover, the PA nanoprobes were found to give high selectivity. The PA signal at 680 nm of nanoprobes incubated with single-base mismatched DNA or other components possibly coexisting with miR-155 in vivo was almost negligible (Figure S6a), demonstrating that the PA signals of the nanoprobes were specifically activated by miR-155. In addition, the PA responses of the nanoprobes to varying concentrations of miR-155 remained unaffected even in fresh serum taken from healthy mice (Figure S6b), indicating the potential of the nanoprobe for in situ PA imaging of miR-155. The optimum volume of PA nanoprobes for miR-155 in situ detection was then studied. For 10 nM miR-155, the PA intensity was saturated when incubated with 50 μg/mL of nanoprobes (Figure S7). And the long-term incubation with PA nanoprobes (50 μg/mL) did not cause apparent cytotoxicity (Figure S8). These nanoprobes are highly sensitive and selective for PA imaging of miR-155 and therefore can be applicable to detecting miR-155 in tumor sites in situ.

In Vivo PA Response of Nanoprobes. After interrogating in vitro response of the nanoprobes, we then explored its ability for in vivo self-assembly and PA response of miR-155. First, we incubated the PA nanoprobes (50 μg/mL) with 4T1 murine breast cancer cells (miR-155 overexpressed, Figure S9). After 1 and 4 h incubation, the cells were collected for TEM analysis. As illustrated in Figure 3a, a majority of the PA nanoprobes were internalized into the interior of cells and accumulated in endosomes or lysosomes after 1 h incubation. When the nanoprobes entered the cytoplasm (4 h), the presence of miR-155 induced the self-assembly of Au aggregates via HCR. In contrast, the single-base mismatched PA nanoprobes (Au-H1*/PEG and Au-H2*/PEG; details of the sequences are shown in Table S1 in the Supporting Information) remained monodisperse during the 4 h incubation period. Similar to cell TEM results, in vivo TEM imaging of 4T1 tumor slices showed that the majority of intratumorally injected PA nanoprobes were taken up by the tumor cells at 1 h. As a result of miR-155 activated-HCR, the perfectly matched nanoprobes successfully assembled into the Au aggregates compared to the control at 4 h postinjection. These experimental results demonstrated the feasibility of the PA nanoprobes for miR-155-selective self-assembly in vivo. Further inspection of the in vivo PA response to miR-155 was performed on 4T1 orthotopic tumor model by intratumoral injection of PA nanoprobes (25 mg/kg). For comparison, the same amount of probes was injected into the muscle on the left leg of this mouse. The PA images given in Figure 3b revealed that, with local injection of perfectly matched nanoprobes, the PA intensity in the tumor was much stronger than that in the muscle. A control group of mice received single-base mismatched PA nanoprobes did not give appreciable PA enhancement. These observations demonstrated that PA activation response was specific to the interaction between miR-155 in tumor and its matched hairpin, not the accumulation of pure AuNPs, validating the high selectivity of the nanoprobes for in vivo PA assay.

Tumor-Penetrating Ability of PA Nanoprobes. Before in vivo tumor miR-155 imaging, we first evaluated the tumor-penetrating ability of the PA nanoprobes. It has been identified that the blood vessels surrounding the tumor are defective and

DOI: 10.1021/acs.analchem.8b01537
Anal. Chem. 2018, 90, 9125−9131

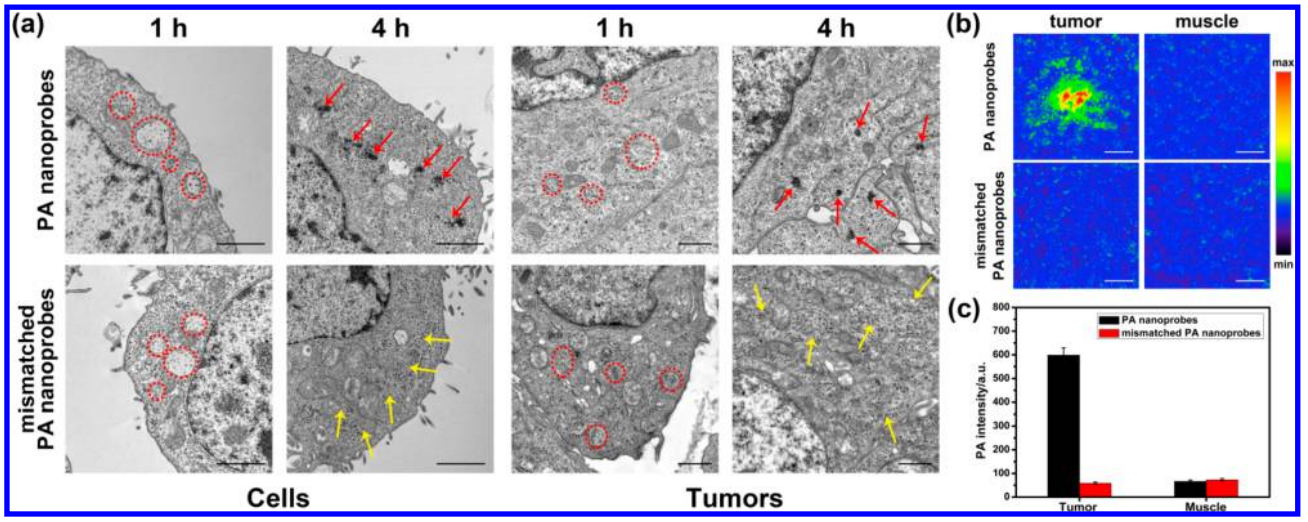

Figure 3. (a) TEM images of the self-assembly process of PA nanoprobes in cells and in tumors. The circles highlight PA nanoprobes taken up into endosomes or lysosomes. The red arrows indicated self-assembled Au aggregates in the cytoplasm. The yellow arrows indicated monodisperse PA nanoprobes. Scale bar = 500 nm. (b) PA imaging of a mouse with its tumor or muscle injected with perfectly matched and single-base mismatched PA nanoprobes. Scale bar = 2 mm. (c) PA intensities of tumor and muscle tissues based on PA imaging data in panel b. Data are shown as mean ± SD (n = 6).

immature.[40] Once a large proportion of the PA nanoprobes were intravenously injected into BALB/c mice bearing 4T1 orthotopic tumors, the leaky vasculature allows them to penetrate and be retained in the tumor bed. To confirm this, tumors and major organs were isolated from mice, and the probe localization was determined by inductively coupled plasma-atomic emission spectroscopy (ICP-AES) at different postinjection times (2, 4, 8, 12, 24, 48, and 168 h). As shown in Figure S10, the PA nanoprobes that relied on EPR effect were accumulated selectively in tumors with maximum value at 8 h postinjection and prolonged tumor retention for 48 h. After 7 days, the Au content decreased in most of the tissues and organs, especially in the heart and kidney demonstrating the safety of the nanoprobes. As a result, the superior EPR effect and reduced potential toxicity of the PA nanoprobes make them highly suitable for the in situ detection of miR-155.

Visualizing miR-155 To Monitor Breast Tumorigenesis by PA Nanoprobes. Have established the tumor penetrating ability of the PA nanoprobes, we next employ them to monitor dynamic changes in miR-155 during breast tumorigenesis. The PA nanoprobes were injected intravenously into BALB/c mice bearing 4T1 orthotopic tumors (dose = 25 mg/kg, n = 6) at different stages (0, 2, 4, 8, 12, 16, and 20 d postinoculation times). To ensure sufficient probe concentration and HCR reaction time, we therefore chose 8 h postinjection to conduct PA imaging to acquire optimal signal (Figure S11). As shown in Figure 4, PA signals of miR-155 at 680 nm were already visible on the second day after tumor inoculation, when the solid tumor had not yet formed. The ability of the nanoprobes to detect this early breast cancer development may be attributed to their EPR effect and the PA signals produced by their self-assembly. The relative PA intensity was calculated by subtracting the preinjection signal intensity from the PA intensity at 8 h postinjection. We found that the PA intensities enhanced steadily during the first 4 days and then intensified rapidly over the next few days (Figure 4b), suggesting that the increased miR-155 levels promoted the formation and growth of tumors (Figure 4c). Although miR-155 levels in tumors were increased consistently, single-base

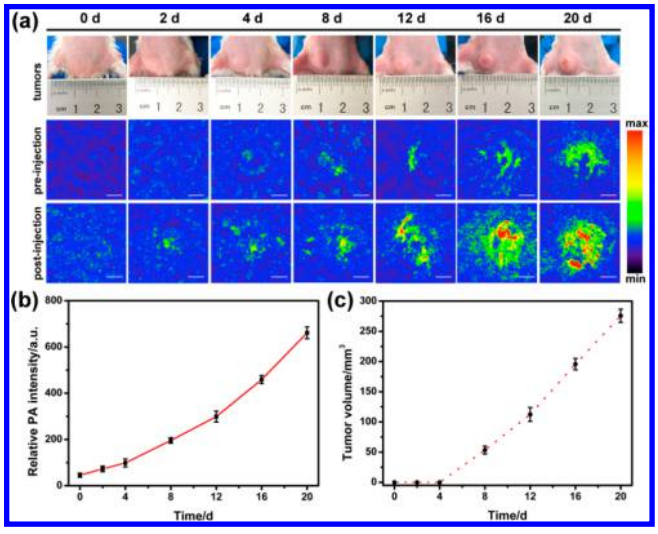

Figure 4. (a) Photographs of tumors and PA monitoring (680 nm pulse laser) of dynamic changes in miR-155 expression levels at different stages (0, 2, 4, 8, 12, 16, and 20 d postinoculation times). Scale bar = 2 mm. (b) Quantification of the PA intensity values in panel a. The relative PA intensity was calculated by subtracting the preinjection signal intensity from the PA intensity at 8 h postinjection. (c) Quantification of the tumor volume at different stages in panel a. Data are shown as mean ± SD (n = 6).

mismatched PA nanoprobes did not give appreciable PA signal enhancement compared to that before injection (Figure S12). These results further demonstrated the specificity of PA680 response to the red-shifting of the miR-155 triggered Au aggregates. The expression level of miR-155 during breast tumorigenesis was also analyzed by qRT-PCR. However, extracting miR-155 from the body is difficult during the first 4 days postinoculation because the solid tumor has not yet formed. As a result, the expression levels of miR-155 in early breast cancer cannot be detected by qRT-PCR, and these levels were not analyzed until 8 days postinoculation (Figure S13). Thus, in contrast with qRT-PCR, the PA nanoprobes not only allow in situ detection of miR-155 during the early stages

DOI: 10.1021/acs.analchem.8b01537
Anal. Chem. 2018, 90, 9125−9131

of breast cancer but can also assist in real-time monitoring of miR-155 during breast tumor growth. Moreover, the PA nanoprobes showed no obvious influence on major organs (analyzed by H&E staining, Figure S14) or the body weight of the mice (Figure S15), suggesting that these biocompatible hypotoxic PA nanoprobes may have great potential for further clinical application in breast cancer via the in situ PA detection of oncogene miR-155.

Visualizing miR-155 To Assess Chemotherapeutic Drug Efficacy by PA Nanoprobes. Considering the significant role and inhomogeneous expression of miR-155 in breast tumorigenesis and development, interfering with expression of miR-155 at different stages of tumor development by chemotherapeutic drugs may have distinct therapeutic effects. We then performed this experiment using DOX as a model drug. DOX binds tightly to DNA and interferes with DNA replication and RNA synthesis causing cancer cell death.[41] According to the characteristics of miR-155 expression during breast tumorigenesis monitored above, the BALB/c mice bearing 4T1 orthotopic tumors were randomly divided into four groups (n = 6). Three groups were treated with DOX via intratumoral injection starting at 0, 4, or 12 d post-inoculation. These mice were given 0.5 mg/kg daily for 4 consecutive days. Another untreated group was set as a control. Then, the dynamic changes of miR-155 and therapeutic effects in each group during the treatment were monitored by PA nanoprobes. In group I, the expression of miR-155 reduced rapidly after 2 days of treatment (beginning the treatment at 0 d postinoculation) and dropped to the lowest level 4 days later (Figure 5a,b). Moreover, it was maintained at this lowest level until the end of the experiment and no tumor was visible (Figure 5a,c). At late stages of inoculation (groups II and III), the DOX-treatment has minor effects on miR-155 expression and tumor growth. The qRT-PCR analysis further verified this (Figure S16). From these data, the therapeutic efficacy of DOX was directly assessed by in situ visualizing miR-155 using our PA nanoprobes. The results showed that DOX inhibits tumor growth by effectively suppressing miR-155 in the early stages of breast cancer, while the drug resistance in tumor cells was apparent with the enhanced miR-155 expression in the later stages. Implication of these results suggests the importance of early diagnosis and treatment for cancer clinically.

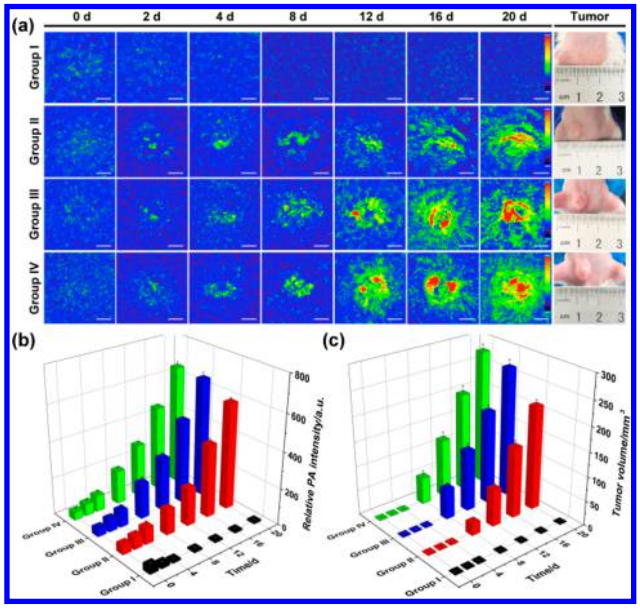

Figure 5. (a) Visualizing miR-155 by PA nanoprobes to assess the chemotherapeutic drug efficacy and photographs of tumors on day 20. Group I, group II, and group III were treated with DOX for 4 consecutive days (0.5 mg/kg daily) starting at 0, 4, or 12 d postinoculation. Untreated group IV was set as a control. Scale bar = 2 mm. (b) Quantification of the PA intensity values in panel a. The relative PA intensity was calculated by subtracting the preinjection signal intensity from the PA intensity at 8 h postinjection. (c) Quantification of the tumor volume at different stages in panel a. Data are shown as mean ± SD (n = 6).

CONCLUSIONS

In summary, a self-assembled HCR-based PA nanoprobe was successfully developed for the first time to monitor dynamic changes in oncogene miR-155 during breast tumorigenesis and chemotherapy. In vitro, the PA nanoprobes achieved highly sensitive and selective quantitative detection of miR-155 with a detection limit of 0.25 nM. Surface modification with PEG and self-assembly of the PA nanoprobes improved resistance to nucleases and the retention time in vivo. Consequently, PA signals of miR-155 could be captured on the second day after tumor inoculation when the solid tumor has not yet formed. The PA intensity also increased as the tumor developed and shows different responses to DOX-treatment at different stages of tumor development, indicating that in situ visualizing miR-155 studies validate the PA nanoprobes as a convenient and reliable way to monitor breast tumorigenesis and response to chemotherapeutic drugs. These findings will be useful in further exploring the mechanism underlying the occurrence, development, and prognosis of breast cancer.

ASSOCIATED CONTENT

Supporting Information

The Supporting Information is available free of charge on the ACS Publications website at DOI: 10.1021/acs.analchem.8b01537.

Experimental details, gel electrophoresis, DLS, ζ potential, nuclease stability, cytotoxicity, biodistribution, PA imaging, qRT-PCR, H&E images, and body weight curves (PDF)

AUTHOR INFORMATION

Corresponding Authors

*E-mail: tangb@sdnu.edu.cn.
*E-mail: gaowen@sdnu.edu.cn.

ORCID

Bo Tang: 0000-0002-8712-7025

Notes

The authors declare no competing financial interest.

ACKNOWLEDGMENTS

This work was supported by the National Natural Science Foundation of China (Grants 21535004, 91753111, 21775092, 21605097, and 21390411) and the Natural Science Foundation of Shandong Province of China (Grant ZR2018JL008).

REFERENCES

(1) Anderson, K. S.; Sibani, S.; Wallstrom, G.; Qiu, J.; Mendoza, E. A.; Raphael, J.; Hainsworth, E.; Montor, W. R.; Wong, J.; Park, J. G.; Lokko, N.; Logvinenko, T.; Ramachandran, N.; Godwin, A. K.; Marks, J.; Engstrom, P.; Labaer, J. *J. Proteome Res.* **2011**, *10*, 85−96.

DOI: 10.1021/acs.analchem.8b01537
Anal. Chem. 2018, 90, 9125−9131

(2) Chapman, C.; Murray, A.; Chakrabarti, J.; Thorpe, A.; Woolston, C.; Sahin, U.; Barnes, A.; Robertson, J. *Ann. Oncol.* **2007**, *18*, 868−873.
(3) Gernaat, S. A. M.; Ho, P. J.; Rijnberg, N.; Lee, S. C.; Lim, S. H.; Yap, Y. S.; Grobbee, D. E.; Hartman, M.; Verkooijen, H. M. *Sci. Rep.* **2017**, *7*, 1365.
(4) Iorio, M. V.; Ferracin, M.; Liu, C. G.; Veronese, A.; Spizzo, R.; Sabbioni, S.; Magri, E.; Pedriali, M.; Fabbri, M.; Campiglio, M.; Menard, S.; Palazzo, J. P.; Rosenberg, A.; Musiani, P.; Volinia, S.; Nenci, I.; Calin, G. A.; Querzoli, P.; Negrini, M.; Croce, C. M. *Cancer Res.* **2005**, *65*, 7065−7070.
(5) Bartel, D. P. *Cell* **2004**, *116*, 281−297.
(6) Lu, J.; Tsourkas, A. *Nucleic Acids Res.* **2009**, *37*, No. e100.
(7) Plasterk, R. H. A. *Cell* **2006**, *124*, 877−881.
(8) Jansson, M. D.; Lund, A. H. *Mol. Oncol.* **2012**, *6*, 590−610.
(9) Hayes, J.; Peruzzi, P. P.; Lawler, S. *Trends Mol. Med.* **2014**, *20*, 460−469.
(10) Kent, O. A.; Mendell, J. T. *Oncogene* **2006**, *25*, 6188−6196.
(11) Zhang, B.; Pan, X.; Cobb, G. P.; Anderson, T. A. *Dev. Biol.* **2007**, *302*, 1−12.
(12) Mattiske, S.; Suetani, R. J.; Neilsen, P. M.; Callen, D. F. *Cancer Epidemiol., Biomarkers Prev.* **2012**, *21*, 1236−1243.
(13) Faraoni, I.; Antonetti, F. R.; Cardone, J.; Bonmassar, E. *Biochim. Biophys. Acta, Mol. Basis Dis.* **2009**, *1792*, 497−505.
(14) Kong, W.; He, L.; Coppola, M.; Guo, J.; Esposito, N. N.; Coppola, D.; Cheng, J. Q. *J. Biol. Chem.* **2010**, *285*, 17869−17879.
(15) Harris, L.; Fritsche, H.; Mennel, R.; Norton, L.; Ravdin, P.; Taube, S.; Somerfield, M. R.; Hayes, D. F.; Bast, R. C. *J. Clin. Oncol.* **2007**, *25*, 5287−5312.
(16) Bertoli, G.; Cava, C.; Castiglioni, I. *Theranostics* **2015**, *5*, 1122−1143.
(17) Yin, J. Q.; Zhao, R. C.; Morris, K. V. *Trends Biotechnol.* **2008**, *26*, 70−76.
(18) Chen, C.; Ridzon, D. A.; Broomer, A. J.; Zhou, Z.; Lee, D. H.; Nguyen, J. T.; Barbisin, M.; Xu, N. L.; Mahuvakar, V. R.; Andersen, M. R.; Lao, K. Q.; Livak, K. J.; Guegler, K. J. *Nucleic Acids Res.* **2005**, *33*, No. e179.
(19) Chapin, S. C.; Appleyard, D. C.; Pregibon, D. C.; Doyle, P. S. *Angew. Chem., Int. Ed.* **2011**, *50*, 2289−2293.
(20) Dong, H.; Lei, J.; Ding, L.; Wen, Y.; Ju, H.; Zhang, X. *Chem. Rev.* **2013**, *113*, 6207−6233.
(21) Liu, H.; Li, L.; Wang, Q.; Duan, L.; Tang, B. *Anal. Chem.* **2014**, *86*, 5487−5493.
(22) Li, L.; Feng, J.; Liu, H.; Li, Q.; Tong, L.; Tang, B. *Chem. Sci.* **2016**, *7*, 1940−1945.
(23) Yang, L.; Ren, Y.; Pan, W.; Yu, Z.; Tong, L.; Li, N.; Tang, B. *Anal. Chem.* **2016**, *88*, 11886−11891.
(24) Smith, A. M.; Mancini, M. C.; Nie, S. *Nat. Nanotechnol.* **2009**, *4*, 710−711.
(25) Liang, C. P.; Ma, P. Q.; Liu, H.; Guo, X.; Yin, B. C.; Ye, B. C. *Angew. Chem., Int. Ed.* **2017**, *56*, 9077−9081.
(26) Triulzi, R. C.; Dai, Q.; Zou, J.; Leblanc, R. M.; Gu, Q.; Orbulescu, J.; Huo, Q. *Colloids Surf., B* **2008**, *63*, 200−208.
(27) Peer, D.; Karp, J. M.; Hong, S.; Farokhzad, O. C.; Margalit, R.; Langer, R. *Nat. Nanotechnol.* **2007**, *2*, 751−760.
(28) Kim, C.; Favazza, C.; Wang, L. V. *Chem. Rev.* **2010**, *110*, 2756−2782.
(29) Wang, S.; Lin, J.; Wang, T.; Chen, X.; Huang, P. *Theranostics* **2016**, *6*, 2394−2413.
(30) Dirks, R. M.; Pierce, N. A. *Proc. Natl. Acad. Sci. U. S. A.* **2004**, *101*, 15275−15278.
(31) Liu, P.; Yang, X.; Sun, S.; Wang, Q.; Wang, K.; Huang, J.; Liu, J.; He, L. *Anal. Chem.* **2013**, *85*, 7689−7695.
(32) Elghanian, R.; Storhoff, J. J.; Mucic, R. C.; Letsinger, R. L.; Mirkin, C. A. *Science* **1997**, *277*, 1078−1081.
(33) Chou, L. Y.; Zagorovsky, K.; Chan, W. C. *Nat. Nanotechnol.* **2014**, *9*, 148−155.
(34) Gao, W.; Zhao, Y.; Li, X.; Sun, Y.; Cai, M.; Cao, W.; Liu, Z.; Tong, L.; Cui, G.; Tang, B. *Chemical Science* **2018**, *9*, 439−445.
(35) McRae Page, S.; Henchey, E.; Chen, X.; Schneider, S.; Emrick, T. *Mol. Pharmaceutics* **2014**, *11*, 1715−1720.
(36) Gao, W.; Sun, Y.; Cai, M.; Zhao, Y.; Cao, W.; Liu, Z.; Cui, G.; Tang, B. *Nat. Commun.* **2018**, *9*, 231.
(37) Gao, J.; Huang, X.; Liu, H.; Zan, F.; Ren, J. *Langmuir* **2012**, *28*, 4464−4471.
(38) Manson, J.; Kumar, D.; Meenan, B. J.; Dixon, D. *Gold Bull.* **2011**, *44*, 99−105.
(39) Pan, C. Q.; Lazarus, R. A. *Biochemistry* **1997**, *36*, 6624−6632.
(40) Maeda, H. *Adv. Enzyme Regul.* **2001**, *41*, 189−207.
(41) Tewey, K. M.; Rowe, T. C.; Yang, L.; Halligan, B. D.; Liu, L. F. *Science* **1984**, *226*, 466−468.

DOI: 10.1021/acs.analchem.8b01537
Anal. Chem. 2018, 90, 9125−9131